RSC Advances

PAPER

View Article Online
View Journal | View Issue

Cite this: *RSC Adv.*, 2021, **11**, 7502

Organic/inorganic double solutions for magnesium–air batteries

Jingling Ma,[abc] Pengfei Hu,*[d] Xingliang Jia,[a] Chenfei Zhang[a] and Guangxin Wang *[a]

In order to limit the anode corrosion and improve the battery activity, magnesium–air batteries with organic/inorganic double solutions (0.5 M $Mg(ClO_4)_2$–*N*,*N*-dimethylformamide (DMF)/0.6 M NaCl–H_2O, 0.5 M $Mg(ClO_4)_2$–acetonitrile (AN)/0.6 M NaCl–H_2O) were prepared. The discharge performance, discharge morphology, and corrosion performance of magnesium anode were researched. Results obtained show that organic electrolytes separate the anode from the aqueous electrolyte, thus improving the anode utilization rate. Due to the NaCl electrolyte used in the air cathode side, batteries show higher discharge voltages. As an example, a better discharge performance has been observed in $Mg(ClO_4)_2$–DMF/NaCl–H_2O double electrolytes at 1 mA cm^{-2} discharge. This is attributed to there being no obvious absorption of corrosion products on the anode surface. The results of the discharge morphology and electrochemical impedance spectroscopy agree well with the discharge performance. The magnesium anode discharge mechanism is different for different solutions.

Received 15th December 2020
Accepted 2nd February 2021

DOI: 10.1039/d0ra10528g

rsc.li/rsc-advances

1 Introduction

Mechanically rechargeable magnesium–air batteries have a high theoretical energy density (3910 W h kg^{-1}) and a high theoretical voltage (3.09 V). Magnesium–air batteries are inexpensive options for applications that require ultrahigh energy densities.[1–3] There is a commercial concern in them as conversion devices, such as off-grid power supplies, long-range drones and electric vehicles.[4,5] The batteries use oxygen in air as the cathode, and the magnesium anode serves as the only active component.[6,7] When the magnesium anode is consumed, the battery continues to discharge by replacing the magnesium anode. Unfortunately, magnesium is a reactive metal and easy to corrode in aqueous solutions. This decreases the anode utilization rate. Magnesium may react with water (reaction (1)), and not produce any current for the circuit.[8,9]

Many papers have focused on reducing the anode corrosion by alloying the magnesium anode,[4,10] and adding corrosion inhibitors in solution to passivate the magnesium surface.[11–13] However, Mg^{2+} cannot penetrate the passivating surface film and corrosion products layer, which obviously inhibits the magnesium dissolution necessary for the magnesium–air battery discharge.[14,15] In addition to alloying and adding corrosion inhibitors, another method is to use an organic electrolyte system.[16,17] According to reports about magnesium corrosion in organic electrolytes,[18–20] the potential of magnesium in dimethylformamide is 2.47 V *versus* Ag/Ag^+.[21] Further, people have investigated the behavior of the magnesium electrode in hexakis (methanol)–dinitrate complex electrolyte[22] and basic electrochemical behavior of Mg^{2+}/Mg couple in organic electrolytes.[23,24]

In this work, organic/inorganic double electrolytes were tested as an alternative method. The double electrolytes consist of an organic electrolyte and an inorganic aqueous electrolyte. The cathodic reaction takes place between the cathode and inorganic electrolyte for the air electrode (reaction (2)), whereas the anodic reaction proceeds between the magnesium electrode and organic electrolyte (reaction (3)). The organic electrolyte, which is immiscible with the inorganic electrolyte, has the function to separate the magnesium anode from the corrosive inorganic electrolyte.

$$Mg + 2H_2O \rightarrow Mg(OH)_2 + H_2 \quad (1)$$

$$O_2 + 2H_2O + 4e^- \rightarrow 4OH^- \quad (2)$$

$$Mg \rightarrow Mg^{2+} + 2e^- \quad (3)$$

In this paper, *N*,*N*-dimethylformamide (DMF: C_3H_7NO) and acetonitrile (AN: C_2H_3N) were selected as the organic solvents. They are good solvents for many substances.[25,26] Inorganic salts are difficult to dissolve in organic solvents, but $Mg(ClO_4)_2$ is soluble in *N*,*N*-dimethylformamide and acetonitrile organic solvents.[27] Therefore, $Mg(ClO_4)_2$ was selected as an ionophore to

[a]*Research Center for High Purity Materials, Henan University of Science and Technology, Luoyang 471023, PR China. E-mail: wanggx2016@126.com; Fax: +86 379 64230597; Tel: +86 379 64231269*

[b]*Collaborative Innovation Center of Nonferrous Metals, Henan Province, Henan University of Science and Technology, Luoyang 471023, PR China*

[c]*Henan Key Laboratory of Non-ferrous Materials Science & Processing Technology, Henan University of Science and Technology, Luoyang 471023, PR China*

[d]*School of Materials Science and Engineering, Luoyang Institute of Science and Technology, Luoyang 471023, PR China*

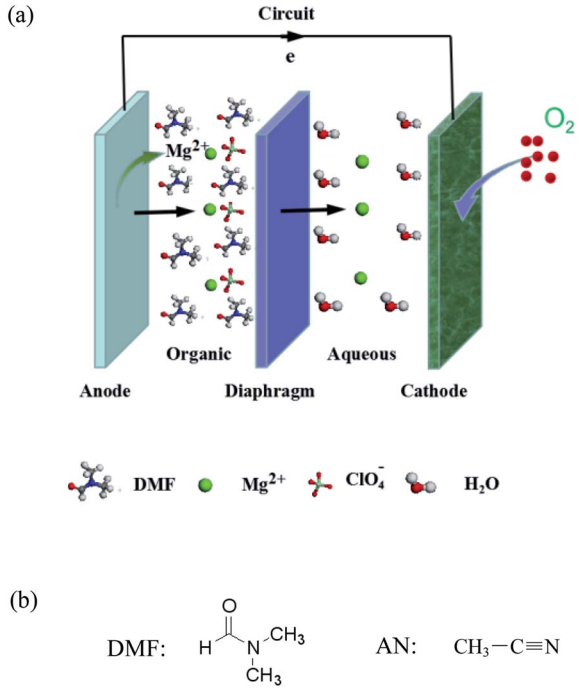

Fig. 1 Schematic of the magnesium–air battery with organic/inorganic double electrolytes (a), and structures of *N*,*N*-dimethylformamide (DMF) and acetonitrile (AN) (b).

transport Mg^{2+}. As the most common electrolyte for the magnesium–air battery, 0.6 M NaCl aqueous solution was used as a cathode electrolyte to keep the battery discharge activity. For the magnesium alloy, aluminum is the most important alloying element. The corrosion is affected strongly by the aluminum content and microstructure. Aluminum is a major alloying element that inhibits corrosion by forming a dense Al_2O_3 protective layer on the alloy surface.[9] The aluminum element in the magnesium alloy can form a β-phase ($Mg_{17}Al_{12}$) if the aluminum content is more than a solid solubility in the α-Mg matrix (maximum solubility is 12.7 wt% at the eutectic temperature 437 °C). Song[15] indicated that the β-phase can serve as an anode barrier to inhibit the corrosion expansion of the α-matrix. As a continuation of earlier research activities,[7,28] Mg–6 wt% Al alloy was selected as the anode material.

Fig. 1a illustrates a schematic of a magnesium–air battery with organic/inorganic double solutions. In organic solution, ClO_4^- plays a charge carrier role. The transfer of Mg^{2+} is accomplished by ion pair ClO_4^- diffusion. ClO_4^- transports Mg^{2+} from the anode into the aqueous solution. In the NaCl aqueous solution, Mg^{2+} moves to the cathode and forms $Mg(OH)_2$ coupled with OH^-. Mg^{2+} migration forms a current. The structures of the organic reagents DMF and AN are presented in Fig. 1b.

2 Experiments

2.1 Material preparation

Commercially pure magnesium and aluminum ingots (99.99%) were used to prepare the Mg–6 wt% Al alloy as the anode material. The ingots were melted under a mixed atmosphere of CO_2 and SF_6 in an induction furnace at 750 °C ± 5 °C. After continuous stirring for 5 min, the molten alloy was poured into a preheated cast iron mold. The actual composition of the alloy was determined by direct reading spectrometry (GS1000, Germany). It contains 5.96 wt% Al, 0.001 wt% Mn, 0.002 wt% Fe, and the rest was Mg. DMF, AN, NaCl, and $Mg(ClO_4)_2$ of analytical grade were purchased from Aladdin. NaCl had no further treatment before its utilization. DMF, AN, and $Mg(ClO_4)_2$ were dried 24 h before use. All weighing and preparation of 0.5 M $Mg(ClO_4)_2$–DMF and 0.5 M $Mg(ClO_4)_2$–AN organic electrolytes were carried out in glove boxes under a highly pure argon atmosphere.

2.2 Electrochemical test

The electrochemical property was tested by a CHI660E equipment with a three-electrode system. The sample of the Mg–6 wt% Al alloy was the working electrode with an exposed area of 1 cm^2. The saturated calomel electrode (SCE) and graphite rod were used as the reference electrode and counter electrode, respectively. Test solutions included 0.6 M NaCl aqueous electrolyte, 0.5 M $Mg(ClO_4)_2$–DMF, and 0.5 M $Mg(ClO_4)_2$–AN organic electrolytes. Electrochemical impedance spectroscopy (EIS) was conducted with a 5 mV sine perturbation from 100 kHz to 0.1 Hz after the working electrode was stable for 1000 s in solution. Potentiodynamic polarization was measured at a scan rate of 1 mV s^{-1} after the sample was stable for 1000 s in the electrolyte. Additionally, the ionic conductivity of different solutions was investigated by the FE38 standard conductivity gauge (Mettler Toledo Instruments Co. Ltd., Switzerland).

2.3 Corrosion test

For the corrosion test, samples of dimension ø 11.3 mm × 5.0 mm were immersed in electrolytes for 5 h. The corrosion products were cleaned out in a solution (200 g L^{-1} CrO_3 + 10 g L^{-1} $AgNO_3$) at 80 °C for 5 min. Weight measurements were made before and after the immersion test to determine the corrosion rate, which is calculated using the following formula:

$$v = \frac{\Delta m}{s \times t} \quad (\text{mg cm}^{-2}\ \text{h}^{-1}) \tag{4}$$

Here, v is the corrosion rate (mg cm^{-2} h^{-1}); Δm is the weight loss (mg); s is the sample surface area (cm^2); and t is the immersion time (h).

2.4 Cell assembly and discharge test

Magnesium–air cells with a single electrolyte and organic/inorganic double electrolytes were assembled. Single electrolytes included 0.6 M NaCl aqueous solution, 0.5 M $Mg(ClO_4)_2$–DMF organic solution, and 0.5 M $Mg(ClO_4)_2$–AN organic solution. The organic/inorganic double electrolytes were 0.5 M $Mg(ClO_4)_2$–DMF/0.6 M NaCl–H_2O and 0.5 M $Mg(ClO_4)_2$–AN/0.6 M NaCl–H_2O. A 20 μm thick hydrophilic treated polypropylene (PP) membrane with a pore diameter <0.1 μm was used as the diaphragm. Polypropylene (PP) as the diaphragm

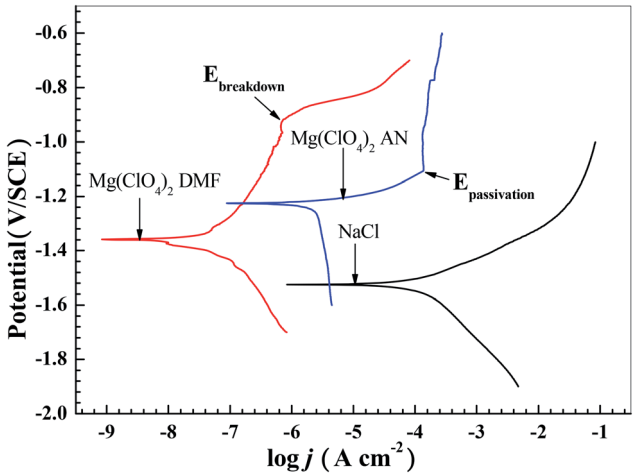

Fig. 2 Polarization curves of the Mg–6 wt% Al alloy in 0.6 M NaCl solution, 0.5 M $Mg(ClO_4)_2$–DMF solution, and 0.5 M $Mg(ClO_4)_2$–AN solution.

has good alkali resistibility, chemical stability, and high air permeability.[29,30] The Mg–6 wt% Al sample with an exposed area of 1 cm^2 acted as the anode. The commercial air cathode with the MnO_2 catalyst was purchased (Changzhou Youteke New Energy Science and Technology, LTD, China). It also had an exposed area of 1 cm^2. Magnesium–air cells were discharged at constant currents of 0.5 mA cm^{-2}, 1 mA cm^{-2}, and 2 mA cm^{-2} for 120 min using a LAND-CT2001A system at room temperature (25 °C ± 5 °C). The anode discharge morphologies before and after cleaning discharge products were analyzed using scanning electron microscopy (SEM : JSM-5610LV) with energy-dispersive X-ray spectroscopy (EDS). The discharge products were cleaned out with a solution of 200 g L^{-1} CrO_3 and 10 g L^{-1} $AgNO_3$ at 80 °C for 5 min. The anode weights before and after discharge were measured to calculate the anode utilization rate according to the formulas (5) and (6):

$$\eta = 100 \times \frac{W}{W_0} \quad (5)$$

Here, η is the anode utilization rate (%), W is the theoretical mass loss, and W_0 is the actual mass loss.

$$W = \frac{Q}{Q_0} \quad (6)$$

Here, Q is the actual current capacity, $Q = 2\ \text{h} \times (0.5, 1, 2)$ mA, and Q_0 is the theoretical current capacity (A h kg^{-1}), $Q_0 = 2219\ \text{A h kg}^{-1} \times 0.94 + 2980\ \text{A h kg}^{-1} \times 0.06 = 2265\ \text{A h kg}^{-1}$.

The anode energy density was calculated using the formula (7):

$$E = \frac{U \times I \times t}{W_0} \quad (7)$$

Here, E is the energy density (W h kg^{-1}), U is the average operating voltage (V), I is the discharge current density (A cm^{-2}), t is the discharge time (h), and W_0 is the actual mass loss (kg).

All of these experiments were repeated at least three times to gauge their reproducibility.

3 Results and discussion

3.1 Potentiodynamic polarization and corrosion

Fig. 2 exhibits the potentiodynamic polarization curves of Mg–6 wt% Al in 0.6 M NaCl electrolyte, 0.5 M $Mg(ClO_4)_2$–DMF electrolyte, and 0.5 M $Mg(ClO_4)_2$–AN electrolyte. The corresponding corrosion parameters are listed in Table 1. The anodic branch does not exhibit Tafel characteristics, and is not as steep as the cathodic branch in Fig. 2. The anodic polarization curves are complicated. Consequently, the Tafel extrapolation for the exchange current density (j_{corr}) calculation can be extrapolated from the cathodic branch to the corrosion potential of the polarization curve.[31] It can be seen that the alloy shows a lower corrosion rate, a lower exchange current density (j_{corr}), a higher polarization resistance (R_p), and a more positive corrosion potential (E_{corr}) in 0.5 M $Mg(ClO_4)_2$–DMF electrolyte and 0.5 M $Mg(ClO_4)_2$–AN electrolyte than in 0.6 M NaCl electrolyte. This indicates that the organic electrolytes can largely decrease the corrosion rate of the alloy, but the alloy becomes slightly less electrochemically active.

In contrast to the polarization curves of the alloy in two organic electrolytes, E_{corr} of the alloy in $Mg(ClO_4)_2$–DMF electrolyte is more negative than in the $Mg(ClO_4)_2$–AN electrolyte, showing that the alloy in the $Mg(ClO_4)_2$–DMF electrolyte possesses a higher activity than in the $Mg(ClO_4)_2$–AN electrolyte. The J_{corr} of the alloy in the $Mg(ClO_4)_2$–DMF electrolyte is lower than in the $Mg(ClO_4)_2$–AN electrolyte, manifesting that the alloy in the $Mg(ClO_4)_2$–DMF electrolyte possesses a lower corrosion rate than in the $Mg(ClO_4)_2$–AN electrolyte. This agrees with the corrosion rate and polarization resistance R_p in Table 1.

3.2 Battery discharge

Fig. 3 exhibits the discharge curves of the magnesium–air batteries in a single electrolyte and organic/inorganic double electrolytes at 0.5 mA cm^{-2}, 1 mA cm^{-2} and 2 mA cm^{-2}. Table 2 presents the discharge parameters of these batteries. Fig. 3a shows the discharge curves at 1 mA cm^{-2} in single electrolytes, including NaCl–H_2O, $Mg(ClO_4)_2$–DMF, and $Mg(ClO_4)_2$–AN

Table 1 Corrosion parameters of Mg–6 wt% Al alloy in 0.6 M NaCl solution, 0.5 M $Mg(ClO_4)_2$–DMF solution, and 0.5 M $Mg(ClO_4)_2$–AN solution

Solutions	E_{corr}/V *vs.* SCE	j_{corr}/mA cm^{-2}	R_p/Ω cm^2	Corrosion rate/mg cm^{-2} h^{-1}	Conductivity rate/ms cm^{-1}
NaCl–H_2O	−1.525	7.55×10^{-3}	2.28×10^2	0.73	51.8
$Mg(ClO_4)_2$–DMF	−1.358	1.37×10^{-6}	6.63×10^5	0.03	21.3
$Mg(ClO_4)_2$–AN	−1.225	5.11×10^{-6}	5.48×10^4	0.05	17.6

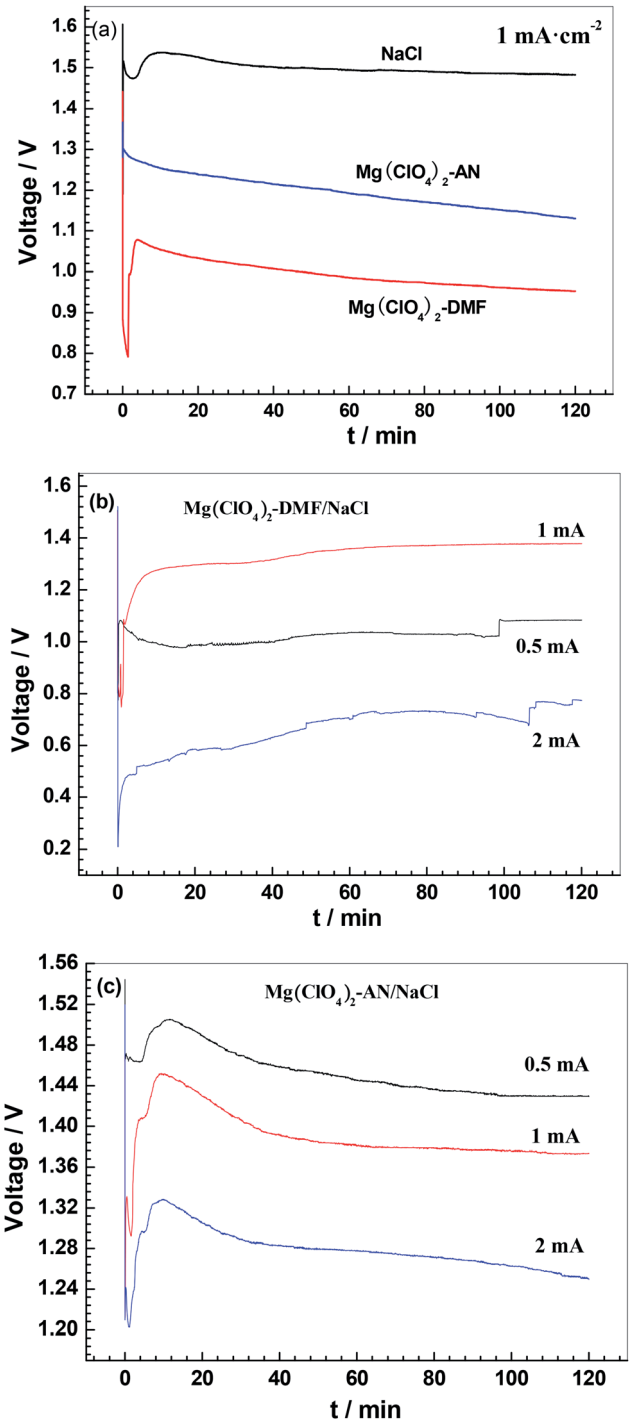

Fig. 3 Discharge curves of the magnesium–air batteries: (a) in single solution at 1 mA cm^{-2}, (b) in 0.5 M $Mg(ClO_4)_2$–DMF/0.6 M NaCl solutions at 0.5 mA cm^{-2}, 1 mA cm^{-2} and 2 mA cm^{-2}, (c) in 0.5 M $Mg(ClO_4)_2$–AN/0.6 M NaCl solutions at 0.5 mA cm^{-2}, 1 mA cm^{-2} and 2 mA cm^{-2}.

electrolytes. The cell average voltage in the NaCl electrolyte is higher than that in organic electrolytes due to the lower conductivity rates of the organic electrolytes (Table 1). The cell voltage drops with increasing discharge time in organic electrolytes. This may be a result of the formation of the adsorption layer on the alloy surface.[32] The anodic utilization rate in the NaCl electrolyte is lower than in both organic electrolytes (Table 2). This is because the alloy violently reacts with water in the NaCl aqueous electrolyte according to reaction (1), producing a large amount of hydrogen. The portion of the alloy consumed in the hydrogen evolution reaction does not proceed to an electricity-producing reaction for the circuit. The Cl^- ions can penetrate the protective $Mg(OH)_2$ film on the alloy electrode surface, and thus promotes corrosion.[31,33] Adopting the $Mg(ClO_4)_2$–DMF electrolyte and $Mg(ClO_4)_2$–AN electrolyte results in a higher anodic utilization rate compared with using the NaCl electrolyte. This might be attributed to the DMF and AN anions adsorbing the anode surface, and there being no water molecules attacking the anode. Using $Mg(ClO_4)_2$–DMF and $Mg(ClO_4)_2$–AN as electrolytes led to higher anodic utilization rates of 85% and 79%, indicating that DMF and AN have an effect of suppressing the corrosion of the magnesium anode. In general, the lower the ionic conductivity rate, the higher the polarization resistance, as can be seen from Table 1. The higher polarization resistance will lead to a strong corrosion resistance, so the anode has a higher utilization rate. The anode utilization rates in organic solutions are higher than in NaCl–H_2O solution.

However, hydrogen evolution caused by the reaction between the magnesium anode and water is not the only reason for the decreased anodic utilization rate. Another reason is that galvanic corrosion between the magnesium matrix and the second phase leads to the dissolution of the magnesium matrix,[34] as shown in Fig. 4d and f. Therefore, in both organic electrolytes, the anode utilization rates are lower than 100%.

Fig. 3b and c show the discharge curves of the magnesium–air batteries with double electrolytes, namely $Mg(ClO_4)_2$–DMF/NaCl–H_2O and $Mg(ClO_4)_2$–AN/NaCl–H_2O. In these batteries, the anodic reaction proceeds in an organic electrolyte, whereas the cathodic reaction proceeds in 0.6 M NaCl–H_2O electrolyte, because the anode contacts with the organic electrolyte, and the air cathode contacts with the NaCl aqueous electrolyte. On the one hand, the organic electrolyte suppresses the anode corrosion. On the other hand, the NaCl aqueous electrolyte can improve the ionic conductivity rate. Therefore, the anodic utilization rates in double electrolytes are in between those of a single organic solution and single NaCl solution (Table 2). It is visible in Fig. 3b that when the discharge starts, the voltage increases slowly as the magnesium electrode activates slowly. At 1 mA cm^{-2}, the average operating voltage, anodic utilization rate, and energy density in the $Mg(ClO_4)_2$–DMF/NaCl–H_2O solutions are 1.358 V, 76%, and 1950 W h kg^{-1}, respectively. The comprehensive discharge performance of the battery at 1 mA cm^{-2} is superior to that at 0.5 mA cm^{-2} and 2 mA cm^{-2} discharge.

In Fig. 3c, the voltage decreases slowly with increasing discharge time. This indicates that there is a competition between the surface adsorption layer and alloy electrode dissolution, with the surface adsorption layer dominating. The surface adsorption layer may be organic magnesium salts and contain O, Mg, Cl, C, and N elements (energy spectral analysis of posts 3 and 4 in Fig. 4e), such as $Mg(N{=}C{=}CH_2)$ (reaction (8)) in the acetonitrile electrolyte. As a result of the surface layer existence, Mg^{2+} cannot pass through this layer. So, the

Table 2 Discharge performance of magnesium–air batteries in 0.6 M NaCl solution, 0.5 M $Mg(ClO_4)_2$–DMF/0.6 M NaCl solutions, and 0.5 M $Mg(ClO_4)_2$–AN/0.6 M NaCl solutions at 0.5 mA cm^{-2}, 1 mA cm^{-2}, and 2 mA cm^{-2}

Solutions	Discharge current/mA cm^{-2}	Average operating voltage/V	Anodic utilization/%	Energy density/W h kg^{-1}	Capacity density/mA h g^{-1}
NaCl	1	1.494	27	905	606
$Mg(ClO_4)_2$–DMF	1	0.986	85	1933	1960
$Mg(ClO_4)_2$–AN	1	1.192	79	1917	1606
$Mg(ClO_4)_2$–DMF/NaCl	0.5	1.036	51	1070	1033
$Mg(ClO_4)_2$–DMF/NaCl	1	1.358	76	1950	1436
$Mg(ClO_4)_2$–DMF/NaCl	2	0.700	80	1799	2570
$Mg(ClO_4)_2$–AN/NaCl	0.5	1.445	47	1103	763
$Mg(ClO_4)_2$–AN/NaCl	1	1.381	52	1463	1059
$Mg(ClO_4)_2$–AN/NaCl	2	1.278	73	1803	1411

magnesium anode dissolution reaction can only proceed when the surface layer breaks down.

$$2CH_3CN + Mg \rightarrow Mg(N_2{=}C{=}CH_2) + H_2 \quad (8)$$

The magnesium–air battery with $Mg(ClO_4)_2$–DMF/NaCl–H_2O double electrolytes has a better discharge performance than that with $Mg(ClO_4)_2$–AN/NaCl–H_2O (Table 2). This may be due to the different performances of DMF and AN. This result is in accordance with the higher activity of the alloy in $Mg(ClO_4)_2$–DMF solution, in contrast to that in the $Mg(ClO_4)_2$–AN solution. The conductivity rate of the $Mg(ClO_4)_2$–DMF electrolyte is higher than that of the $Mg(ClO_4)_2$–AN electrolyte (Table 1). The polarization curve of the alloy in the $Mg(ClO_4)_2$–DMF electrolyte (Fig. 2) shows a passivation section in the anode branch. When the alloy contacts with organic solutions, complicated reactions take place. These reactions result in the formation of a surface adsorption layer. However, the over potentials of several tens of millivolts are enough to break down the adsorption layer.[32] Then, the current increases sharply. The corresponding potential is the breakdown potential ($E_{breakdown}$). The polarization curve of the alloy in the $Mg(ClO_4)_2$–AN electrolyte also shows a passivation section and a signal passivation potential ($E_{passivation}$) in the anode branch (Fig. 2). However, with increasing potential, the current shows almost no change, and $E_{breakdown}$ does not appear. This indicates that the adsorption layer is difficult to break down in the $Mg(ClO_4)_2$–AN electrolyte. At present, there are few studies on the magnesium–air battery with double solutions. Magnesium–air batteries with butyl butyrate-20 wt% [BMIM][TFSI]/10 wt% $Mg(TFSI)_2$–H_2O double solutions were reported by Wu Zr *et al.*[35] At 0.6 mA cm^{-2} discharge, the magnesium–air battery showed 91.6% anodic utilization rate, 2020 mA h g^{-1} capacity density, and 0.7 V operating voltage. Due to the different double solution systems, paper[35] showed the lower operating voltage, but a higher anodic utilization rate and capacity density. However, the ionic liquid [BMIM][TFSI] was very expensive.

3.3 Discharge morphology

Fig. 4 presents the SEM images of the Mg–6 wt% Al anodes after discharge at 1 mA cm^{-2} in NaCl–H_2O electrolyte, $Mg(ClO_4)_2$–DMF/NaCl–H_2O electrolytes, and $Mg(ClO_4)_2$–AN/NaCl–H_2O electrolytes. Images without cleaning discharge products are shown in Fig. 4a, c and e, whereas images with discharge products being cleaned out are shown in Fig. 4b, d and f. The anode surface is covered by thick discharge products after discharge in the NaCl electrolyte (Fig. 4a). Fig. 5 shows the XRD analysis of the Mg–6 wt% Al alloy after discharge in 0.6 M NaCl solution without cleaning out the discharge product. It mainly contains $Mg(OH)_2$ and NaCl. This indicates that the main discharge products are $Mg(OH)_2$ in NaCl electrolyte, and the NaCl phase in XRD is the dried up NaCl electrolyte. After cleaning the discharge products, some cracks and pits are visible (Fig. 4b). This illustrates that a serious local corrosion took place, which leads to a lower anodic utilization rate in the NaCl solution (Table 2). Many turtle shell-shapes with little cracks are visible on the anode surface after discharge in 0.5 M $Mg(ClO_4)_2$–DMF/NaCl–H_2O solutions (Fig. 4c). The turtle shell-shaped cracks indicate that the discharge products easily break down. After cleaning out, some shallow corrosion pits and scratches made by abrasive paper are visible on the anode surface (Fig. 4d). This means that the anode corrosion occurs very little in the $Mg(ClO_4)_2$–DMF/NaCl–H_2O solutions. The anode discharged in 0.5 M $Mg(ClO_4)_2$–AN/NaCl–H_2O solutions (Fig. 4e) has fewer discharge products and scratches on its surface, and some shallow pitting and scratches are observed clearly after cleaning out (4f). The discharge products in $Mg(ClO_4)_2$–DMF/NaCl–H_2O and $Mg(ClO_4)_2$–AN/NaCl–H_2O are too little to collect, and cannot be determined using XRD. Fig. 4c and e show the EDS analysis on the corroded surface of the alloy after discharge. The discharge products at positions 1 and 2, positions 3 and 4 all contain O, Mg, Cl, C, and N elements in $Mg(ClO_4)_2$–DMF/NaCl–H_2O and $Mg(ClO_4)_2$-AN/NaCl–H_2O solutions. The O, Mg, and Cl elements may be the dried up $Mg(ClO_4)_2$ electrolyte. The C and N elements indicate that DMF and AN react with the alloy, or adsorb on the alloy surface. In contrast, there is no H element on the alloy surface. This is because the H element has only one extranuclear electron, and it is not possible to detect it by EDS.

Comparing the discharge morphologies in Fig. 4, one can see that the anode is severely corroded in the NaCl electrolyte, while the anode is only slightly corroded in the organic/NaCl double

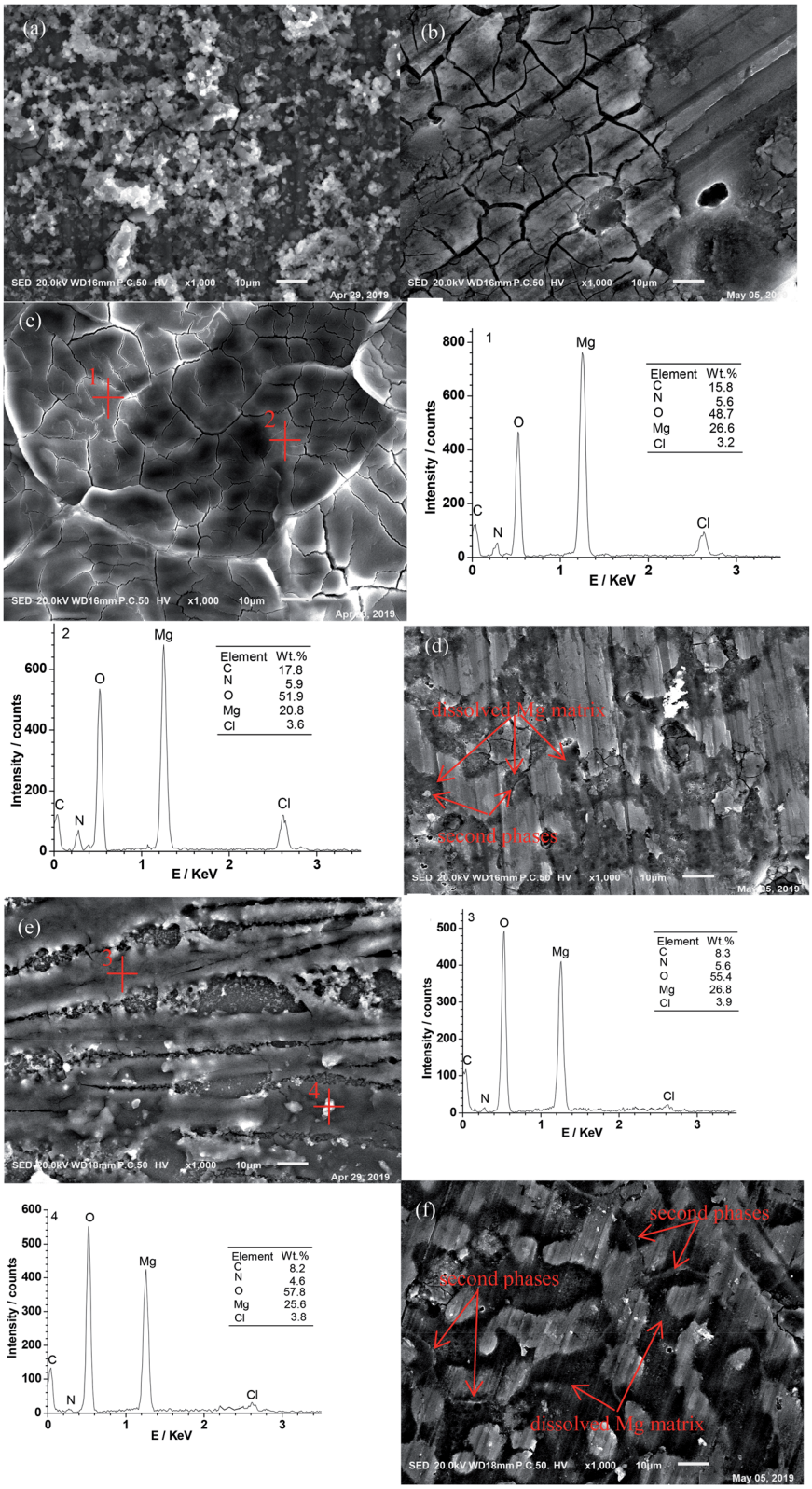

Fig. 4 SEM of the Mg–6 wt% Al alloy after discharge in different solutions before cleaning out the corrosion product: 0.6 M NaCl (a), 0.5 M $Mg(ClO_4)_2$–DMF/0.6 M NaCl–H_2O (c), 0.5 M $Mg(ClO_4)_2$–AN/0.6 M NaCl–H_2O (e), and after cleaning out the corrosion product: 0.6 M NaCl (b), 0.5 M $Mg(ClO_4)_2$–DMF/0.6 M NaCl–H_2O (d), 0.5 M $Mg(ClO_4)_2$–AN/0.6 M NaCl–H_2O (f), energy spectral analysis of post 1 and 2 of (c), and post 3 and 4 of (e).

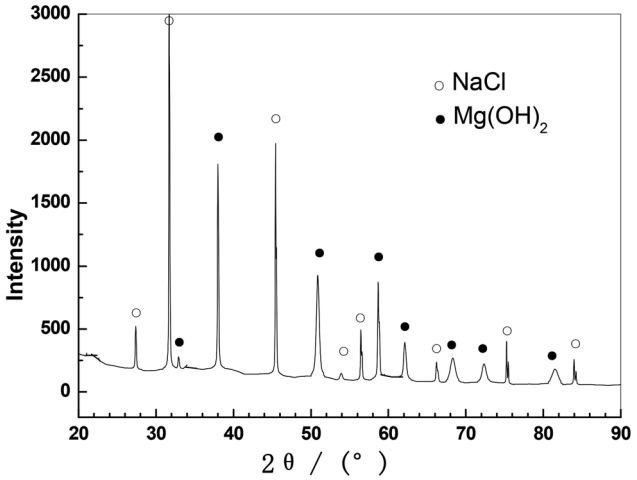

Fig. 5 XRD of the Mg–6 wt% Al alloy after discharge in 0.6 M NaCl solution without cleaning out the discharge product.

solutions. As a consequence, the batteries have a higher anodic utilization rate and a higher energy density in the organic/NaCl double solutions (Table 2). As a comparison of the anode discharge images produced in the two double solutions (see Fig. 4c and e), only a thin layer of discharge products with cracks can be seen on the anode surface after discharge in the $Mg(ClO_4)_2$–DMF/NaCl–H_2O electrolytes (Fig. 4c). In contrast, obvious discharge products can be seen after discharge in the $Mg(ClO_4)_2$–AN/NaCl–H_2O electrolytes (Fig. 4e). This indicates that the anode discharged in the $Mg(ClO_4)_2$–DMF/NaCl electrolytes has less corrosion than the one discharged in the $Mg(ClO_4)_2$–AN/NaCl–H_2O electrolytes. In Fig. 4d and f, some shallow pitting corrosion is visible on the anode surfaces. The shallow pitting corrosion is believed to be due to the dissolution of the magnesium matrix, which can result from the galvanic corrosion between the magnesium matrix and the second phases of the magnesium alloy.[36,37] There are some grey and white precipitated phases and some shallow corrosion pits due to the dissolved magnesium matrix observed in Fig. 4d and f. Galvanic corrosion has occurred between the precipitated phases and magnesium matrix. The magnesium matrix is dissolved as an anode. The precipitated phases as cathodes are not eroded. However, due to the dissolution of the magnesium matrix surrounding the precipitated phases, this causes some precipitated phases to fall off.

3.4 EIS

Fig. 6a presents the electrochemical impedance spectra of Mg–6 wt% Al in the NaCl electrolyte. Two capacitive arcs appear at high frequency and at medium frequency, respectively, and an inductive arc appears at lower frequency. The fitted curves match well with the experimental data (Fig. 6a). An equivalent circuit is shown in Fig. 6a, containing R_s, R_t and CPE_t, R_f and CPE_f, R_1 and L_1.[38,39] R_s is the solution resistance. The high frequency capacitive arc is because of the Mg–Mg^{2+} reaction. Equivalent components contain R_t (charge transfer resistance) and CPE_t (double-layer capacitance). The controlling step is the

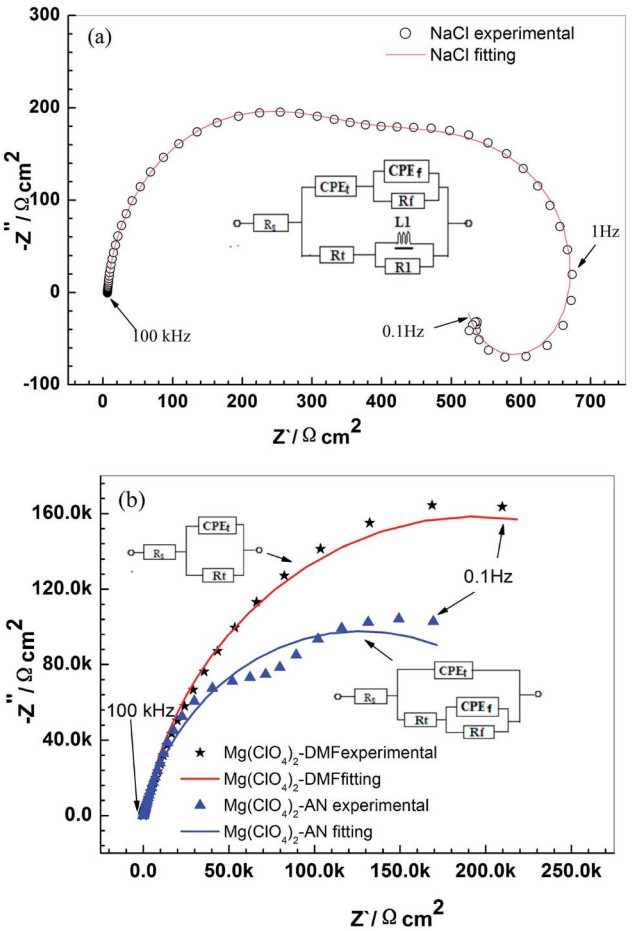

Fig. 6 EIS spectra of the Mg–6 wt% Al alloy in 0.6 M NaCl solution (a), 0.5 M $Mg(ClO_4)_2$–DMF solution, and 0.5 M $Mg(ClO_4)_2$–AN solution (b).

charge transfer process. The medium frequency capacitive arc is due to the absorption of the corrosion products on the anode surface. CPE_f and R_f are the capacitance and resistance of the absorption layer, respectively. The lower frequency inductive arc is due to the local corrosion on the anode surface, as shown in Fig. 4b.[40–42] L_1 and R_1 are the inductance and resistance of the corrosion reaction (reaction (1)), respectively. According to Fig. 6a, the anode corrosion occurs mainly *via* magnesium dissolution (Mg–Mg^{2+}) and local corrosion in the NaCl electrolyte.

The EIS of the alloy in the $Mg(ClO_4)_2$–DMF electrolyte and $Mg(ClO_4)_2$–AN electrolyte is shown in Fig. 6b. There is only a capacitive arc at high frequency in the $Mg(ClO_4)_2$–DMF electrolyte. An equivalent circuit according to Fig. 6b contains R_s, R_t and CPE_t. Then, the anode corrosion occurs mainly *via* magnesium dissolution (Mg–Mg^{2+}) in the $Mg(ClO_4)_2$–DMF electrolyte. Two capacitive arcs appear at high frequency and at medium frequency in the $Mg(ClO_4)_2$–AN electrolyte, respectively. An equivalent circuit is shown in Fig. 6b, containing R_s, R_t and CPE_t, R_f and CPE_f. Anode corrosion occurs mainly *via* magnesium dissolution (Mg–Mg^{2+}) and the absorption of corrosion products in $Mg(ClO_4)_2$–AN electrolyte. From Fig. 6b for the anode discharged in organic electrolytes, the inductive

Table 3 EIS simulated values of Mg–6 wt% Al alloy in 0.6 M NaCl solution, 0.5 M $Mg(ClO_4)_2$–DMF solution, and 0.5 M $Mg(ClO_4)_2$–AN solution

Solutions	NaCl	$Mg(ClO_4)_2$/DMF	$Mg(ClO_4)_2$/AN
$R_s/\Omega\ cm^2$	6.5	21.7	12.17
$CPE_t/\Omega^{-1}\ cm^{-2}\ s^{-1}$	7.92×10^{-6}	3.32×10^{-6}	2.34×10^{-6}
$n_t/0 < n < 1$	0.9	0.87	0.90
$R_t/\Omega\ cm^2$	392.6	3.89×10^5	6.28×10^3
$CPE_f/\Omega^{-1}\ cm^{-2}\ s^{-1}$	2.28×10^{-4}	—	1.46×10^{-6}
$N_f/0 < n < 1$	0.8	—	0.70
$R_f/\Omega\ cm^2$	122.6	—	2.53×10^5
$L_1/H\ cm^2$	42.56	—	—
$R_1/\Omega\ cm^2$	213.7	—	—

arc as a symbol of local corrosion is too slight to appear in EIS (Fig. 6b). This shows that the local corrosion is slight in organic electrolytes. For the anode tested in the $Mg(ClO_4)_2$–DMF electrolyte, a medium frequency capacitive arc as a symbol of the absorption of corrosion products does not appear. This manifests that there is no absorption layer in the $Mg(ClO_4)_2$–DMF electrolyte, and the alloy has a higher activity in the $Mg(ClO_4)_2$–DMF electrolyte than in the $Mg(ClO_4)_2$–AN electrolyte. The results of EIS agree well with the discharge morphology in Fig. 4.

Table 3 shows the fitting values obtained by ZSimpwin software, according to the equivalent circuit. R_t of 392.6 $\Omega\ cm^2$, $3.89 \times 10^5\ \Omega\ cm^2$, and $6.28 \times 10^3\ \Omega\ cm^2$ are gained for tests in the NaCl electrolyte, $Mg(ClO_4)_2$–DMF electrolyte, and $Mg(ClO_4)_2$–AN electrolyte, respectively. R_t in organic electrolytes is much large than that in NaCl electrolyte. This indicates a lower corrosion rate in the organic electrolytes than in NaCl electrolyte. The result is consistent with the corrosion rate in Table 1 and the discharge morphology in Fig. 4.

4 Conclusions

Based on the results obtained in this study, the following conclusions can be drawn for magnesium–air batteries with organic/inorganic double electrolytes:

(1) Using organic electrolytes to separate the anode from the corrosive aqueous electrolyte can improve the anodic utilization rate.

(2) A better discharge performance can be achieved for magnesium–air batteries with 0.5 M $Mg(ClO_4)_2$–DMF/0.6 M NaCl–H_2O double electrolytes.

(3) A higher discharge voltage can be obtained when using the aqueous NaCl electrolyte in the air cathode side.

Conflicts of interest

There are no conflicts of interest to declare.

Acknowledgements

This work was supported by the Chinese 1000 Plan for High Level Foreign Experts (grand no. WQ20154100278), and the National Natural Science Foundation (grant no. U1804146).

References

1 F. W. Richey, B. D. McCloskey and A. C. Luntz, Mg anode corrosion in aqueous electrolytes and implications for Mg–air batteries, *J. Electrochem. Soc.*, 2016, **163**, A958–A963.
2 N. N. Xu, Q. Nie, L. Y. Q. Luo, C. Z. Yao, Q. J. Gong, Y. Y. Liu, X. D. Zhou and J. L. Qiao, Controllable hortensia-like MnO_2 synergized with carbon nanotubes as an efficient electrocatalyst for long-term metal–air batteries, *ACS Appl. Mater. Interfaces*, 2019, **1**, 578–587.
3 Z. Ma, D. R. Farlane and M. Kar, Mg Cathode Materials and Electrolytes for Rechargeable Mg Batteries: A Review, *Batteries Supercaps*, 2019, **2**, 1–14.
4 Q. Zhang, J. Chen and Q. A. Li, Strength stability of aging hardened Mg-10Y-1.5Sm alloy, *Rare Met. Mater. Eng.*, 2018, **47**(3), 799–802.
5 Y. P. Wu, Z. F. Wang, Y. Liu, G. F. Li, S. H. Xie, H. Yu and H. Q. Xiong, AZ61 and AZ61-La alloys as anodes for Mg–air battery, *J. Mater. Eng. Perform.*, 2019, **28**, 2006–2016.
6 A. P. Shyma, S. Palanisamy, N. Rajendhran and R. Venkatachalam, Enhanced discharge capacity of Mg–air battery with addition of water dispersible nano MoS_2 sheet in $MgCl_2$ electrolyte, *Ionics*, 2019, **25**, 583–592.
7 Y. Q. Li, J. L. Ma, G. X. Wang, F. Z. Ren, Y. J. Zhu, Y. F. Song and J. L. Zhang, Effect by adding Ce and In to Mg–6Al Alloy as anode on performance of Mg–air batteries, *Mater. Res. Express*, 2019, **6**, 066315.
8 X. Liu, J. L. Xue and S. Z. Liu, Discharge and corrosion behaviors of the alpha-Mg and beta-Li based Mg alloys for Mg–air batteries at different current densities, *Mater. Des.*, 2018, **160**, 138–146.
9 A. Pardo, M. C. Merino, A. E. Coy, F. Viejo, R. Arrabal and S. Feliú, Influence of microstructure and composition on the corrosion behaviour of Mg/Al alloys in chloride media, *Electrochim. Acta*, 2008, **53**, 7890–7902.
10 X. Liu, J. L. Xue and D. Zhang, Electrochemical behaviors and discharge performance of the as-extruded Mg-1.5 wt% Ca alloys as anode for Mg–air battery, *J. Alloys Compd.*, 2019, **790**, 822–828.
11 Y. C. Zhao, G. S. Huang, G. L. Gong, T. Z. Han, D. B. Xia and F. S. Pan, Improving the intermittent discharge performance of Mg–air battery by using oxyanion corrosion inhibitor as electrolyte additive, *Acta Metall. Sin.*, 2016, **29**, 1019–1024.
12 J. L. Zhang, J. L. Ma, G. X. Wang, Y. Q. Li and A. A. Volinsky, Electrochemical performance of 1-ethyl-3-methylimidazolium bis(trifluoromethylsulfonyl) imide ionic liquid as electrolyte for primary Mg air batteries, *J. Electrochem. Soc.*, 2019, **166**, A1103–A1106.
13 S. Y. Liew, J. C. Juan, C. W. Lai, G. T. Pan, T. C. K. Yang and T. K. Lee, An eco-friendly water-soluble graphene-incorporated agar gel electrolyte for magnesium–air batteries, *Ionics*, 2019, **25**, 1291–1301.
14 N. G. Wang, Y. C. Mu, W. H. Xiong, J. C. Zhang, Q. Li and Z. C. Shi, Effect of crystallographic orientation on the discharge and corrosion behaviour of AP65 magnesium alloy anodes, *Corros. Sci.*, 2018, **144**, 107–126.
15 G. L. Song and A. Atrens, Corrosion mechanisms of magnesium alloys, *Adv. Eng. Mater.*, 1999, **1**, 11–18.

16 A. R. Polu and R. Kumar, Preparation and characterization of PEG–$Mg(CH_3COO)_2$–CeO_2 composite polymer electrolytes for battery application, *Bull. Mater. Sci.*, 2014, **37**(2), 309–314.

17 D. Lu, H. Q. Liu, T. Huang, Z. X. Xu, L. Ma, P. Yang, P. R. Qiang, F. Zhang and D. Q. Wu, Magnesium ion based organic secondary batteries, *J. Mater. Chem. A*, 2018, **6**, 17297–17302.

18 M. A. Deyab, Decyl glucoside as a corrosion inhibitor for magnesiumeair battery, *J. Power Sources*, 2016, **325**, 98–103.

19 Y. S. He, Q. Li, L. L. Yang, C. R. Yang and D. S. Xu, Electrochemical-conditioning-free and water-resistant hybrid $AlCl_3/MgCl_2/Mg(TFSI)_2$ electrolytes for rechargeable magnesium batteries, *Angew. Chem.*, 2019, **58**, 7615–7619.

20 H. J. Lee, J. Shin and J. W. Choi, Intercalated water and organic molecules for electrode materials of rechargeable batteries, *Adv. Mater.*, 2018, **30 SI**.

21 R. Manjuladevi, S. Selvasekarapandian, M. Thamilselvan, R. Mangalam, S. Monisha and P. C. Selvin, A study on blend polymer electrolyte based on poly(vinyl alcohol)–poly (acrylonitrile) with magnesium nitrate for magnesium battery, *Ionics*, 2018, **24**, 3493–3506.

22 E. Sheha and M. El-Deftar, Magnesium hexakis(methanol)–dinitrate complex electrolyte for use in chargeable magnesium batteries, *J. Solid State Electrochem.*, 2018, **22**, 2671–2679.

23 C. S. Li, Y. Sun, F. Gebert and S. L. Chou, Current progress on rechargeable magnesium–air battery, *Adv. Energy Mater.*, 2017, **7**, SI.

24 N. Wang, Y. N. NuLi, S. J. Su, J. Yang and J. L. Wang, Effects of binders on the electrochemical performance of rechargeable magnesium batteries, *J. Power Sources*, 2017, **341**, 219–229.

25 M. Konni, A. S. Dadhich and S. B. Mukkamala, Solvent induced surface modifications on hydrogen storage performance of ZnO nanoparticle decorated MWCNTs, *Sustainable Energy Fuels*, 2017, **2**, 466–471.

26 L. Yang, J. S. Dordick and S. Garde, Hydration of enzyme in nonaqueous media is consistent with solvent dependence of its activity, *Biophys. J.*, 2004, **87**, 812–821.

27 O. R. Brown and R. Mcuntyre, The magnesium and magnesium amalgam electrodes in aprotic organic solvents:a kinetic study, *Electrochim. Acta*, 1985, **30**, 627–633.

28 Y. F. Song, J. L. Ma, Y. Q. Li, G. X. Wang, C. H. Qin and H.-R. Stock, Effects of second phases in anode materials on discharge performance of Mg–air batteries, *Ionics*, 2019, **25**, 5899–5906.

29 L. Stano, M. Stano and P. Durina, Separators for alkaline water electrolysis prepared by plasma-initiated grafting of acrylic acid on microporous polypropylene membranes, *Int. J. Hydrogen Energy*, 2020, **45**, 80–93.

30 A. Ratner, R. Beaumont and I. Masters, Dynamic Mechanical Compression Impulse of Lithium-Ion Pouch Cells, *Energies*, 2020, **13**, 2105, DOI: 10.3390/en13082105.

31 J. R. Li, Q. T. Jiang, H. Y. Sun and Y. T. Li, Effect of heat treatment on corrosion behavior of AZ63 magnesium alloy in 3.5% sodium chloride solution, *Corros. Sci.*, 2016, **111**, 288–301.

32 D. Aurbach, Y. Gofer, A. Schechter, O. Chusid, H. Gizbar, Y. Cohen, M. Moshkovich and R. Turgeman, A comparison between the electrochemical behavior of reversible magnesium and lithium electrodes, *J. Power Sources*, 2001, **97–98**, 269–273.

33 M. Deng, D. Hoche, S. V. Lamaka, D. Snihirova and M. L. Zheludkevich, Mg–Ca binary alloys as anodes for primary Mg–air batteries, *J. Power Sources*, 2018, **396**, 109–118.

34 J. L. Ma, G. X. Wang, Y. Q. Li, C. H. Qin and F. Z. Ren, Electrochemical Investigations on AZ Series Magnesium Alloys as Anode Materials in a Sodium Chloride Solution, *J. Mater. Eng. Perform.*, 2019, **28**, 2883–2870.

35 Z. J. Wang, Y. Q. Niu, Z. Wu, *et al.*, Double liquid electrolyte for primary Mg batteries, *J. Power Sources*, 2014, **247**, 840–844.

36 J. L. Ma, Y. Zhang, M. S. Ma, C. H. Qin, F. Z. Ren and G. X. Wang, Corrosion and discharge performance of a magnesium aluminum eutectic alloy as anode for magnesium–air batteries, *Corros. Sci.*, 2020, **4**, 108695.

37 S. M. Li, H. Q. Qian and L. Qin, The analysis of the volume ratio of oxide on the alloy, *Corros. Sci. Prot. Technol.*, 1999, **11**(5), 284–289.

38 J. L. Ma, J. B. Wen, Q. A. Li and Q. Zhang, Electrochemical polarization and corrosion behavior of Al–Zn–In based alloy in acidity and alkalinity solutions, *Int. J. Hydrogen Energy*, 2013, **38**, 14896–14902.

39 J. L. Ma, F. Z. Ren, W. H. Li, G. X. Wang, Y. Xiong, Y. Q. Li and J. B. Wen, Electrochemical performance of melt-spinning Al–Mg–Sn based anode alloys, *Int. J. Hydrogen Energy*, 2017, **42**, 11654–11661.

40 J. L. Ma, Y. Zhang, C. H. Qin, F. Z. Ren and G. X. Wang, Effects of polystyrene sulfonate/graphene and Mn_3O_4/graphene on property of aluminum(zinc)–air batteries, *Int. J. Hydrogen Energy*, 2020, **45**, 13025–13034.

41 Y. Yang, F. Scenini and N. Stevens, *et. al.*, Relationship between the inductive response observed during electrochemical impedance measurements on aluminium and local corrosion processes, *Corros. Eng., Sci. Technol.*, 2019, **54**, 1521591, DOI: 10.1080/1478422X.2018.1521591.

42 D. Mareci, G. Bolat and J. Izquierdo, *et. al.*, Electrochemical characteristics of bioresorbable binary MgCa alloys in Ringer's solution: Revealing the impact of local pH distributions during *in vitro* dissolution, *Mater. Sci. Eng., C*, 2016, **60**, 402–410.